MCN

Molecular and Cellular Neuroscience **17,** 274–291 (2001)
doi:10.1006/mcne.2000.0939, *available online at http://www.idealibrary.com on* IDEAL®

Complex Genetic Interactions among Four Receptor Tyrosine Phosphatases Regulate Axon Guidance in *Drosophila*

Qi Sun,[1] Benno Schindelholz, Matthias Knirr,[2] Aloisia Schmid, and Kai Zinn

Division of Biology, California Institute of Technology, Pasadena, California 91125

Four receptor-linked protein tyrosine phosphatases are selectively expressed on central nervous system axons in the *Drosophila* embryo. Published data show that three of these (DLAR, DPTP69D, DPTP99A) regulate motor axon guidance decisions during embryonic development. Here we examine the role of the fourth neural phosphatase, DPTP10D, by analyzing double-, triple-, and quadruple-mutant embryos lacking all possible combinations of the phosphatases. This analysis shows that all four phosphatases participate in guidance of interneuronal axons within the longitudinal tracts of the central nervous system. In the neuromuscular system, DPTP10D works together with the other three phosphatases to facilitate outgrowth and bifurcation of the SNa nerve, but acts in opposition to the others in regulating extension of ISN motor axons past intermediate targets. Our results provide evidence for three kinds of genetic interactions among the neural tyrosine phosphatases: partial redundancy, competition, and collaboration.

INTRODUCTION

Receptor-linked protein tyrosine phosphatases (RPTPs) are important regulators of axon guidance decisions in *Drosophila* embryos and larvae. In the embryo, the functions of the RPTPs have been primarily studied in the neuromuscular system, which contains a small number of motor neurons whose axons can be easily visualized by antibody staining. In each abdominal segment (A2–A7) of the embryo, 32 motor axons exit the central nervous system (CNS) within the ISN (intersegmental nerve) and SN (segmental nerve) roots and then split into five pathways that innervate 30 muscle fibers. The SNa and SNc pathways emerge from the SN root, and the ISN, ISNb, and ISNd pathways arise from the ISN root (ISNb and ISNd are also known as SNb and SNd). The stereotyped and relatively simple nature of the neuromuscular system makes it possible to analyze how specific genes regulate the formation of individual synapses (for review see Keshishian *et al.,* 1996).

Five *Drosophila* RPTP genes have been described thus far; these encode DPTP4E, DPTP10D, DLAR, DPTP69D, and DPTP99A (Hariharan *et al.,* 1991; Oon *et al.,* 1993; Streuli *et al.,* 1989; Tian *et al.,* 1991; Yang *et al.,* 1991). Our analysis of the complete *Drosophila* sequence (Adams *et al.,* 2000) suggests that there is only one additional RPTP encoded in the genome (B.S. and K.Z., unpublished). Remarkably, four of the five known RPTPs are selectively expressed on CNS axons (Desai *et al.,* 1994; Hariharan *et al.,* 1991; Tian *et al.,* 1991; Yang *et al.,* 1991). DPTP4E mRNA is expressed in the CNS and in several other tissues; this RPTP has not been genetically characterized, however, and its protein distribution pattern has not been determined (Oon *et al.,* 1993). The four "neural" RPTPs DPTP10D, DLAR, DPTP69D, and DPTP99A have been studied using genetics. All four phosphatases regulate axon guidance decisions in the embryo (Desai *et al.,* 1996, 1997; Krueger *et al.,* 1996; Sun *et al.,* 2000).

Single mutants lacking DLAR or DPTP69D display altered guidance of ISNb axons in the neuromuscular system (Desai *et al.,* 1996; Krueger *et al.,* 1996). Many motor axon pathway decisions, however, are altered only when specific combinations of two or more RPTPs are eliminated. For example, when DLAR, DPTP69D, and DPTP99A are all absent, the ISN is unable to extend

[1] Present address: Proteome, Inc., 100 Cummings Center, Suite 420B, Beverly, MA 01915.

[2] Present address: FB Biology, Chemistry, Pharmacy, Freie Universitat Berlin, Takustrasse 3, 14195 Berlin, Germany.

1044-7431/01 $35.00

beyond its first intermediate target. When only DLAR and DPTP69D are missing, the ISN stalls at its second intermediate target (Desai *et al.*, 1997). No visible alterations in the embryonic CNS or neuromuscular system are detected in single mutants lacking DPTP10D or DPTP99A (Desai *et al.*, 1996; Sun *et al.*, 2000). These results correlate with the observation that *Dlar* and *Ptp69D* mutations confer lethality, while *Ptp10D* and *Ptp99A* null mutants are viable and fertile.

Genetic studies also indicate that RPTPs can have opposing activities (in a formal genetic sense). DLAR and DPTP99A function in opposition to each other in regulating entry of the ISNb into its target ventrolateral muscle (VLM) field (Desai *et al.*, 1997). The Abl tyrosine kinase also opposes the activity of DLAR at this choice point (Wills *et al.*, 1999).

In third-instar larvae, DPTP69D is required for innervation of the lamina of the optic lobe by photoreceptor neurons. When DPTP69D is not expressed on photoreceptor (R) axons, the growth cones of R1–6 photoreceptors fail to stop at their lamina targets and continue into the medulla. R7 axons also make targeting errors. Phosphatase activity and extracellular domain sequences are both required for DPTP69D function in the optic lobes (Garrity *et al.*, 1999) (Newsome *et al.*, 2000).

We recently described the isolation of mutations in the gene encoding the fourth neural RPTP, DPTP10D. Analysis of these mutations shows that RPTPs are also essential for interneuronal axon guidance within the CNS (Sun *et al.*, 2000). This had not been apparent before now because loss of all three of the other neural RPTPs (DLAR, DPTP69D, and DPTP99A) does not have a strong effect on the CNS axonal array (Desai *et al.*, 1997; see below). Removal of DPTP10D and DPTP69D, however, generates a unique CNS phenotype in which many extra axons cross the midline. The *Ptp10D Ptp69D* double mutation interacts with *roundabout* (*robo*), *commissureless* (*comm*), and *slit*, a set of mutations defining a repulsive pathway that prevents longitudinal axons from crossing the midline (reviewed by Zinn and Sun, 1999). In this paper, we define the roles of the four neural RPTPs in controlling motor and CNS axon guidance by analyzing the phenotypes of all double, triple, and quadruple mutants.

RESULTS

Sequence Requirements for DPTP69D Function in the CNS

Ptp10D Ptp69D mutant embryos have a unique CNS phenotype in which longitudinal axons abnormally cross the midline (Sun *et al.*, 2000) (Fig. 1E). This phenotype can be observed using mAb 1D4, which recognizes three longitudinal bundles on each side of the CNS in late stage 16 and early stage 17 embryos (Van Vactor *et al.*, 1993). There is little staining in the commissures at these stages in wild-type embryos (Figs. 1A and 1B). Thus, abnormal midline crossing by 1D4-positive axons in *Ptp10D; Ptp69D* mutants can be easily visualized as commissural 1D4 staining (Fig. 1E, arrow). Greater than 95% of segments have 1D4-positive commissural bundles in these mutants (Sun *et al.*, 2000).

The existence of this highly penetrant double-mutant phenotype made it possible to address sequence requirements for RPTP function in the embryonic CNS. Garrity *et al.* (1999) used GAL4-driven *Ptp69D* transgenes (Brand and Perrimon, 1993) to rescue the *Ptp69D* optic lobe phenotype. We crossed the same transgenes into the *Ptp10D; Ptp69D* mutant background, together with panneuronal GAL4 sources (*Elav-GAL4*), and evaluated the fraction of embryos that displayed the characteristic double mutant CNS phenotype. These data show that the requirements for DPTP69D sequences in rescuing the embryonic CNS phenotype are the same as for phenotypic rescue in the optic lobe (Garrity *et al.*, 1999). Within the extracellular domain, the fibronectin type III (FN3) repeats are required, but the immunoglobulin-like (Ig) domains are not. Mutants in which either the first or the second cytoplasmic PTP domain is inactivated or deleted are still able to rescue. If inactivating point mutations are introduced into the active sites of both PTP domains, however, the resulting DPTP69D construct does not rescue the double-mutant phenotype (Table 1).

Removal of DPTP10D Reveals Distinct Roles for All Four Neural RPTPs in Control of CNS Axon Guidance

To study the roles of the four RPTPs in regulating axon guidance in the embryo, we generated and analyzed double-, triple-, and quadruple-mutant embryos lacking DPTP10D and one or more of the other three neural RPTPs. These embryos were recognized by the lack of staining with monoclonal antibodies (mAbs) against each of the RPTPs (see Experimental Methods). To simplify the analysis, we used a single combination of null mutations for each of the RPTPs. For *Ptp69D*, *Ptp99A*, and *Dlar* (denoted in Flybase as *Lar*), we employed null transheterozygous mutant combinations previously used by Desai *et al.* (1997) to define the roles of these three RPTPs in motor axon guidance; this allowed direct comparison of our results with theirs (see

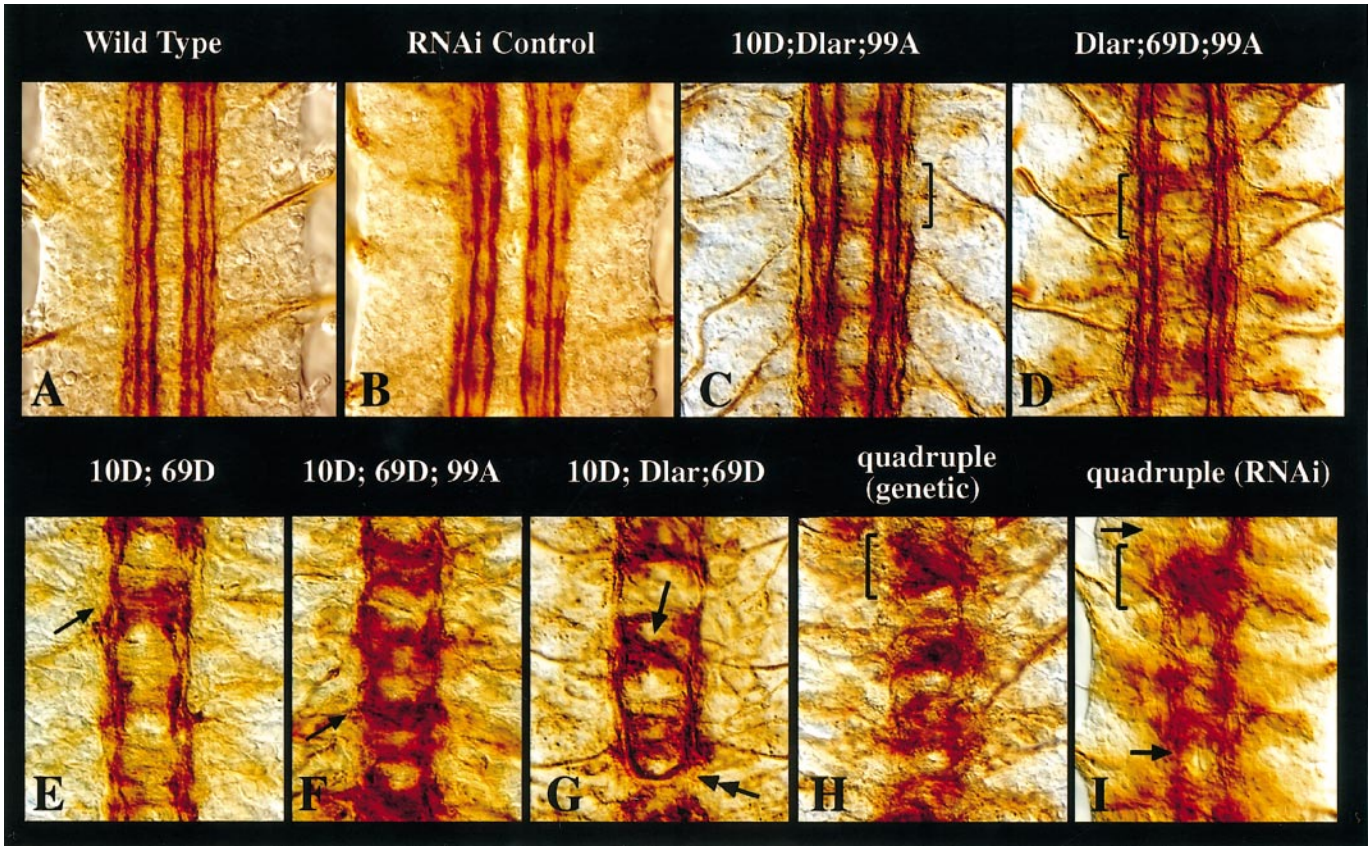

FIG. 1. CNS phenotypes in *Rptp* mutant embryos. (A–I) The CNS of dissected late stage 16 embryos stained with mAb 1D4. (A) Wild type. Note the three continuous longitudinal bundles on each side of the CNS and the lack of 1D4-staining axons in the commissural tracts. (B) RNAi control. An embryo injected with buffer at the blastoderm stage and allowed to develop to stage 16. (C) *Ptp10D; Dlar; Ptp99A*. The inner bundles are normal, but the outer bundle is discontinuous (bracket). (D) *Dlar; Ptp69D; Ptp99A*. The phenotype is similar to that of *Ptp10D; Dlar; Ptp99A*. A gap in the outer bundle is indicated (bracket). (E) *Ptp10D; Ptp69D*. The outer bundles are fused, so that only one or two are present, and many stained axons cross the midline (arrow). (F) *Ptp10D; Ptp69D; Ptp99A*. Similar to *Ptp10D; Ptp69D*, but more longitudinal bundle fusion is observed, and more axons cross the midline (arrow). (G) *Ptp10D; Dlar; Ptp69D*. The longitudinal tracts are fused. A whole tract may be rerouted diagonally across the midline (arrow) or may cross the midline and circle back into the contralateral longitudinal tract, producing a complete connective break (double arrow). (H) *Ptp10D; Dlar; Ptp69D; Ptp99A* (genetic). The longitudinal connectives are disrupted, and many thick bundles cross the midline to form a fused 1D4-positive commissural tract in each segment (bracket). (I) *Ptp10D; Dlar; Ptp69D; Ptp99A* (RNAi). Wild-type blastoderm embryos were injected with a mixture of dsRNAs for each of the four RPTPs and allowed to develop to stage 16. A phenotype like that of the quadruple genetic mutant is observed, with fused 1D4-positive commissures (bracket) and frequent connective breaks (arrows).

Experimental Methods for details). *Ptp10D* is on the X chromosome, so it is most straightforward to examine hemizygous males when examining *Ptp10D* mutant phenotypes. We were able to do this using the null allele $Ptp10D^{1}$, because it is hemizygous/homozygous viable and fertile and has a small molecularly characterized deletion that affects only the *Ptp10D* gene (Sun *et al.*, 2000; also analyzed further using the complete *Drosophila* genome sequence). We had previously shown that two other independently generated *Ptp10D* alleles produce the same phenotypes as $Ptp10D^{1}$ when combined with *Ptp69D* (Sun *et al.*, 2000).

None of the *Rptp* combinations, including the quadruple mutation, produce muscle or peripheral nervous system abnormalities (data not shown). This is consistent with the observation that no expression of any of the four RPTPs can be detected on muscles or sensory neurons (Tian *et al.*, 1991; Yang *et al.*, 1991; Hariharan *et al.*, 1991; Desai *et al.*, 1994, 1996; Krueger *et al.*, 1996).

To investigate how RPTPs regulate guidance of 1D4-positive axons within the CNS, we analyzed the phenotypes of all triple mutants. We found that late stage 16 triple mutants lacking DLAR, DPTP69D, and DPTP99A, although they have very severe motor axon

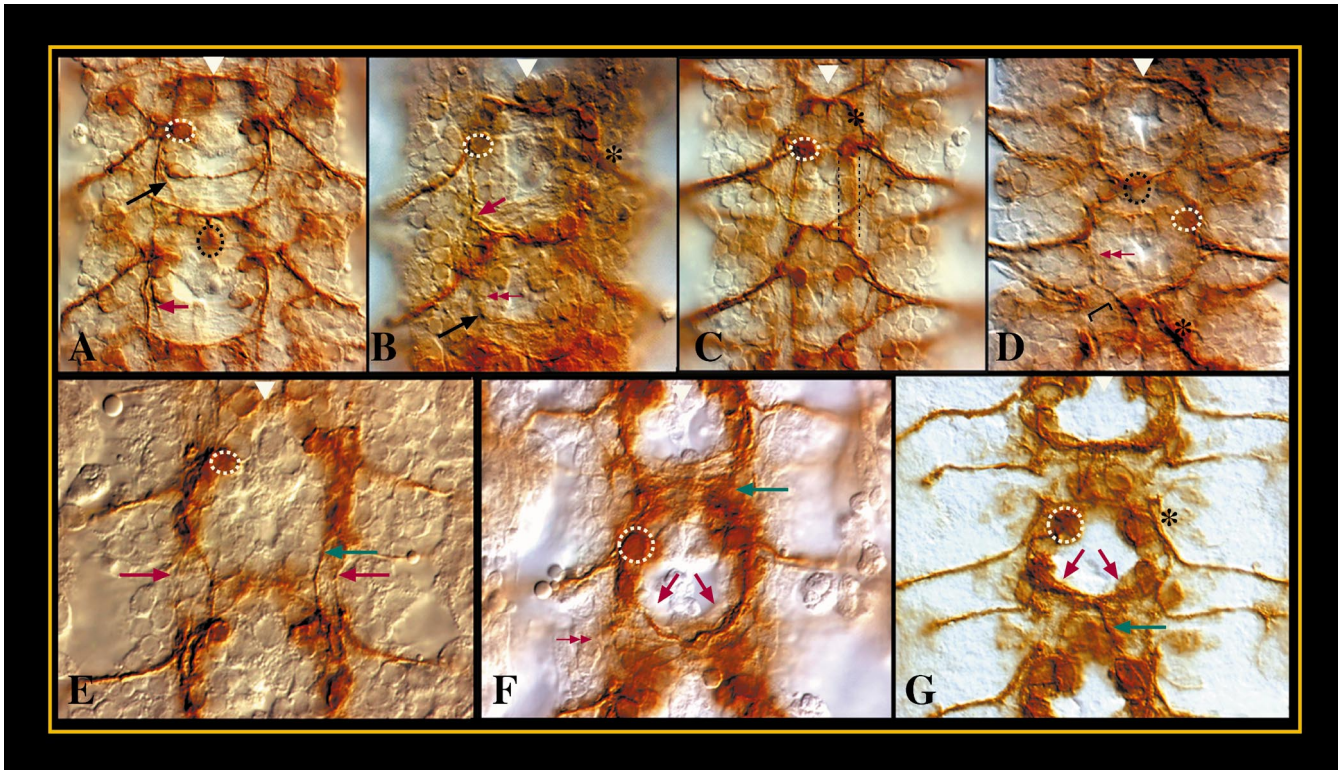

FIG. 2. Removal of all four RPTPs affects pioneer axon pathways. (A–D) Late stage 13 (A, B) and late stage 15/early stage 16 (C, D) embryonic CNS preparations stained with mAb 22C10. (A) and (C) are wild-type embryos, and (B) and (D) are embryos injected with dsRNAs for all four RPTPs. (E–G) Stage 13 embryonic CNS preparations stained with mAb 1D4. (E) is an RNAi control embryo injected with buffer, (F) is a quadruple RNAi embryo injected with dsRNAs for all four RPTPs, and (G) is a *robo* embryo. Black arrows: SP1 pathways. Red arrows: MP1/dMP2 pathways. Green arrows: pCC/vMP2 pathways. Double red arrows: missing pathways (MP1/dMP2 in (B), pCC/vMP2 in (F), late longitudinal 22C10 pathway in (D)). White dotted outlines: aCC cell bodies. Black dotted outlines: VUM cell bodies. Asterisks: RP cell bodies. Dotted straight lines in (C) define the late longitudinal 22C10 pathway. Bracket in (D) indicates missing RP axons on one side. The RP pathway on the contralateral side is thicker than normal. Note the similar curvatures of the MP1/dMP2 pathway to the midline in (F) and (G).

defects (Desai *et al.*, 1997), do not display strong CNS phenotypes that are detectable with this marker. Like wild-type embryos, they have distinct longitudinal 1D4-positive bundles and little commissural staining. The morphologies of the two inner bundles are very similar to that of wild type, but the outer bundle, which develops later, is often discontinuous (Fig. 1D, bracket). When DPTP10D, DLAR, and DPTP99A are all absent, a similar CNS phenotype is observed. Again, the two inner bundles are intact, while the outer bundle is discontinuous (Fig. 1C, bracket). In rare segments of these embryos, the inner bundle contacts the midline. These results show that CNS longitudinal 1D4-positive bundles avoid the midline in a normal manner when either DPTP10D *or* DPTP69D is expressed and all three of the other RPTPs are absent.

Removal of DPTP10D, DPTP69D, and DPTP99A produces a phenotype similar to, but more severe than, that of *Ptp10D; Ptp69D* (Sun *et al.*, 2000), in which the three longitudinal bundles are partially fused and many 1D4-positive axons cross the midline (Figs. 1E and 1F, arrows). Thus, removal of DPTP99A strengthens the basic phenotype produced by the absence of DPTP10D and DPTP69D.

The *Ptp10D; Dlar; Ptp69D* triple mutant also has a strong phenotype involving ectopic midline crossing and longitudinal bundle fusion (Fig. 1G). It differs from the *Ptp10D; Ptp69D; Ptp99A* phenotype, however, in that the axons that abnormally cross the midline in these embryos often grow diagonally to the other side without respecting the normal borders of the anterior and posterior commissures. In many cases, all of the 1D4-positive connective axons appear to be rerouted across the midline, producing complete connective breaks (Fig. 1G, double arrow).

Finally, when all four RPTPs are absent, a phenotype

TABLE 1
Functional Analysis of *Ptp69D* Mutants

	Transgene[a]	Percentage of expected phenotype (*n*)[b]	Rescue[c]
	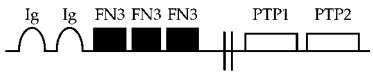		
Extracellular domain mutants			
69DD (Ig)	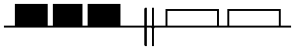	7.2 (469)	+
69DD (FNIII)	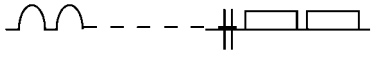	85.6 (450)	–
69D/EC (RPTPμ)		100.0 (288)	–
Intracellular domain mutants			
69D (wedge)		21.6 (623)	+
69D (DA1)		6.7 (301)	+
69DD (PTP2)		15.2 (312)	+
69D (DA1DA2)		98.4 (447)	–

[a] Transgenes were driven in all postmitotic neurons using *Elav-GAL4*.
[b] Number of embryos showing midline crossing phenotype compared to the number of embryos expected to show the phenotype (transgene on X chromosome, 25%; transgene on second or third chromosome, 12.5%). *n*, number of embryos examined.
[c] "+" denotes that the transgene rescued the *Ptp10D; Ptp69D* phenotype (<25% of the expected number embryos display the phenotype). "–" indicates failure to rescue (>75% of the expected number of embryos display the phenotype).

is observed in which most of the 1D4 axons cross the midline and the longitudinal 1D4 bundles are almost absent (Figs. 1H and 1I). Staining of these quadruple-mutant embryos with mAb BP102, which recognizes all CNS axons, shows that the longitudinal tracts are depleted of axons and that the commissures are completely fused (bracket) and much thicker than normal (Sun *et al.*, 2000). Taken together, these results suggest that in the absence of all four neural phosphatases, most of the pathways in the longitudinal tracts are converted into commissural pathways that cross the midline (compare Figs. 1A and 1H). In summary, the RPTPs display a remarkable specificity in regulating CNS axon guidance; loss of any two or three of the four does not strongly affect the two inner 1D4-positive bundles unless both DPTP10D and DPTP69D are missing.

Longitudinal Pioneer Axons Cross the Midline in Embryos Lacking All Four RPTPs

Staining with mAb 1D4 at late stages does not permit visualization of the trajectories of individual axons. By examining earlier (stage 13) embryos, we have previously shown that longitudinal pioneer axons are not strongly affected in *Ptp10D; Ptp69D* double-mutant embryos (Sun *et al.*, 2000). The longitudinal 1D4-positive axons that cross the midline or follow other abnormal pathways in these embryos appear later (stage 15), and they cannot be individually visualized because of the large number of pathways that are stained with the mAb by this time. We were, however, able to observe individual axons abnormally crossing the midline in *Ptp10D; Ptp69D* mutants by examining neuronal lineages deriving from single DiI-labeled neuroblasts (NBs; see Schmid *et al.*, 1999). For example, the NB 2–5 progeny axons normally cross the midline once and extend anteriorly along the contralateral longitudinal connective. In *Ptp10D; Ptp69D* mutants, they double back across the midline after crossing once and then grow posteriorly in the ipsilateral connective (Sun *et al.*, 2000).

Since quadruple mutants lacking all four neural RPTPs have a very strong phenotype in which all 1D4-positive axons appear to cross the midline, we antici-

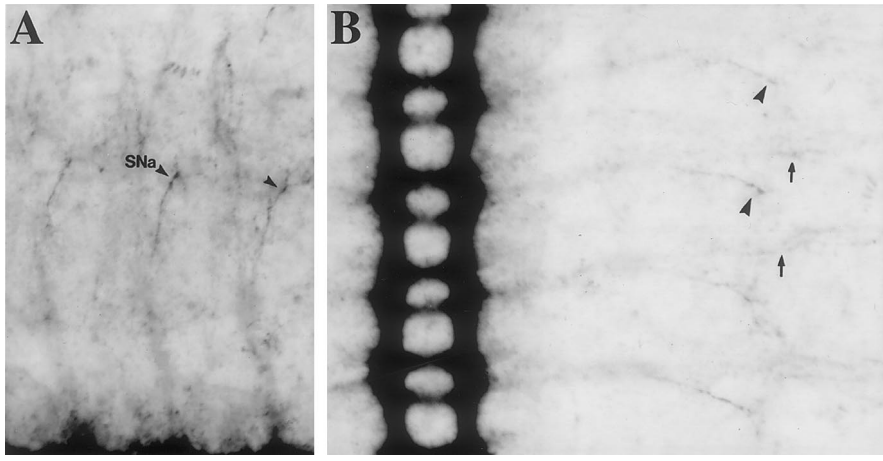

FIG. 3. Expression of DPTP10D in the CNS and on the SNa nerve. (A) A bright-field photograph of a hemisegment of a late stage 14 embryo stained with an anti-DPTP10D mAb. The CNS is the darkly stained region at the bottom. At this stage, the only motor pathway that can be visualized with this mAb is the SNa nerve, whose growth cones are just above the arrowheads. The right-hand SNa has just bifurcated. (B) A lower magnification bright-field photograph of the same embryo, showing the CNS and the entire periphery. SNa branches are indicated (arrowheads). The arrows indicate tracheal branches, which also appear to stain weakly at this time in development.

pated that longitudinal pioneer axons should be affected in this genotype. Unfortunately, it is not possible to identify quadruple mutant embryos (1/128 of the total) at stage 13 by the absence of staining with mAbs against the four RPTPs, because staining is too weak at this stage. One also cannot use marked balancers to identify these embryos, because the *Rptp* genes are on all three chromosomes and triply balanced stocks cannot be maintained. Accordingly, we had to develop a new technique to generate and study early quadruple-mutant embryos. To do this, we used RNAi methods, which have been shown to be effective in inhibiting gene expression in *Drosophila* embryos (Kennerdell and Carthew, 1998; Misquitta and Paterson, 1999). We have been able to obtain effective inhibition of the expression of two, three, or four RPTPs simultaneously by injecting the appropriate concentrations of double-stranded RNAs (dsRNAs) into blastoderm embryos (A.S., B.S., and K.Z., unpublished; see Experimental Methods). A complete description of these methods will be published elsewhere. In Fig. 1B, we show that embryos injected with buffer and allowed to develop to stage 16 or17 have a 1D4 staining pattern that is indistinguishable from that of wild type. Embryos injected with dsRNAs for all four of the neural RPTPs have a CNS phenotype at late stage 16 that closely resembles that of quadruple genetic mutants (Fig. 1I). These embryos also display motor axon phenotypes that are indistinguishable from those of quadruple mutants (data not shown; see Figs. 4–6 for quadruple-mutant motor axon phenotypes).

In early stage 13 embryos, only one longitudinal pathway is stained by mAb 1D4. This contains the axons of the MP1, dMP2, vMP2, and pCC neurons. In wild-type embryos, the MP1 and dMP2 axons fasciculate with each other and extend posteriorly, while the vMP2 and pCC axons fasciculate and extend anteriorly. The ascending and descending axons meet to form a continuous longitudinal pathway (Fig. 2E; Seeger *et al.*, 1993). This pathway then splits into two separate bundles: pCC/vMP2 (green arrow) and MP1/dMP2 (red arrow) (Hidalgo and Brand, 1997). In *Ptp10D; Ptp69D* mutants, these two pioneer pathways form in an apparently normal manner (Sun *et al.*, 2000).

The longitudinal pioneer axons are diverted across the midline in *robo* embryos, in which axonal repulsion from the midline is reduced (Kidd *et al.*, 1998a,b). The initial trajectory of the pCC/vMP2 axons is altered, so that they grow diagonally to the midline (Fig. 2G, green arrow) and then cross. The MP1/dMP2 axons begin to extend posteriorly in a normal manner, but then curve across the midline (red arrows).

In quadruple RNAi embryos (Fig. 2F, red arrows), we observe that the MP1/dMP2 axons usually follow a curving pathway to the midline, as they do in *robo* embryos. In some segments, the ascending pCC/vMP2 axons grow anteriorly to establish a longitudinal pathway to the next segment (green arrow). In others, they stall, leading to the formation of a break in the 1D4-positive connective (double red arrow). They seldom, however, grow diagonally to the midline as they do in *robo* mutants (Fig. 2G, green arrow).

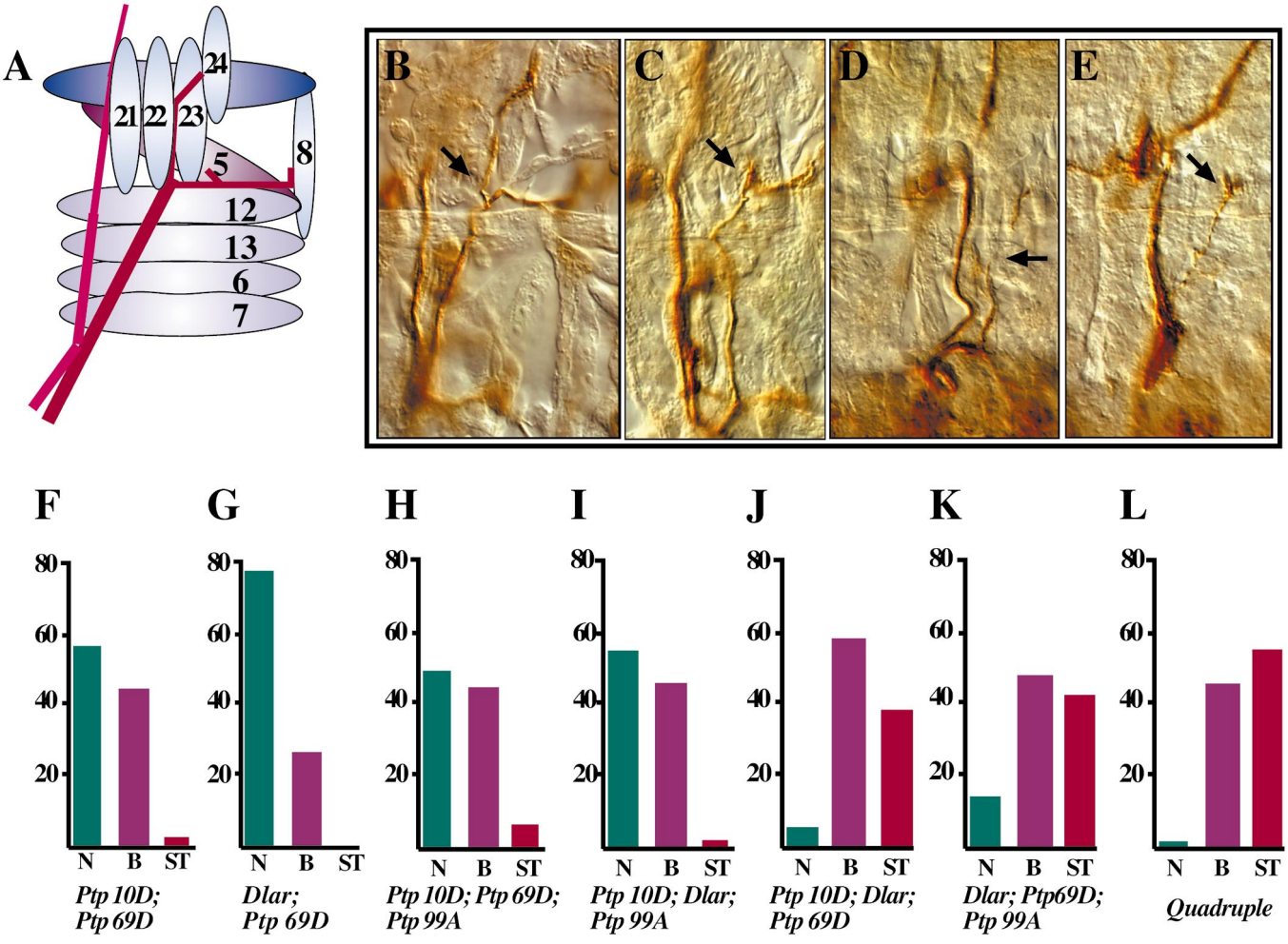

FIG. 4. SNa phenotypes in *Rptp* mutant embryos. (A) Schematic diagram of the SNa nerve and surrounding muscles. SNa is shown in purple, and the ISN is shown in red. The SNa usually bifurcates at the cleft between muscles 22 and 23, and it innervates muscles 5, 8, and 21–24. (B–E) Each image shows a hemisegment of a late stage 16 embryo stained with mAb 1D4. Arrows in (B), (C), and (E) mark the approximate points at which SNa would normally bifurcate; arrow in (D) marks the truncation point of the main SNa nerve. One or a few axons grow beyond this point and form the stained synaptic segment above the arrow. (B) Wild type. (C) *Ptp10D; Ptp69D*. The anterior SNa branch is missing. (D) An abnormally short SNa, in a quadruple mutant. (E) A very thin SNa that stops around the bifurcation point, also in a quadruple mutant. (F–L) Bar graphs showing the SNa phenotypes of different mutant combinations. The ordinates represent the penetrances (in % of hemisegments) of the various phenotypes. N (green bars): normal SNa. B (purple bars): SNa reaches the bifurcation point, but is missing one or both branches. ST (red bars): SNa is either very short or very thin. *n* values (number of abdominal segments (A2–A7) scored): F, 130; G, 118; H, 117; I, 107; J, 106; K, 111; L, 71.

We also observed alterations in pioneer pathways using a different marker, the 22C10 mAb (Zipursky *et al.*, 1984). At stage 13, this mAb stains the ascending vMP2 and SP1 axons, the descending MP1 and dMP2 axons, and the bifurcating VUM axons, among others (Seeger *et al.*, 1993). The SP1 axons cross the midline and fasciculate with the vMP2 axons; thus, in wild-type embryos a curving SP1 pathway crossing the midline that meets the longitudinal MP1 pathway is seen (Fig. 2A, black arrow). In quadruple RNAi embryos, the MP1/dMP2 axons curve toward the midline (red arrow). In the segment shown, the MP1/dMP2 axons appear to be crossing the midline at the anterior–posterior position of the VUM and RP axons.

The bilateral RP(1,3,4) group of motor neurons sends axons across the midline. These contact the contralateral RP cell bodies, then grow posteriorly and exit the CNS in the ISN root. In quadruple RNAi embryos, the RP cell bodies are often displaced (Fig. 2B, asterisk), and

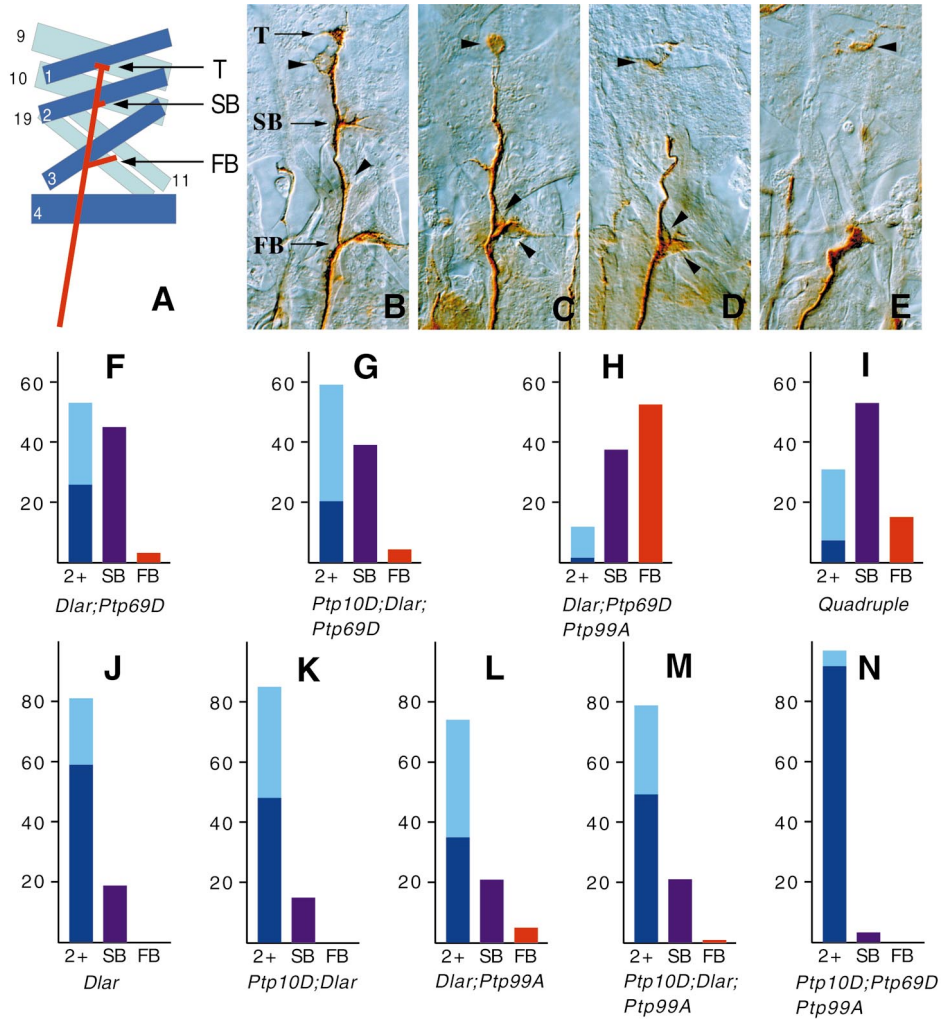

FIG. 5. ISN phenotypes in *Rptp* mutant embryos. (A) A schematic diagram of a late stage 16 ISN and some of its surrounding target muscles. The first (FB) and second (SB) lateral branch points and the terminal arbor (T) are indicated. (B–E) Each image shows a late stage 16/early stage 17 ISN stained with mAb 1D4. Three different kinds of phenotypes are represented. The arrowheads indicate persistent twist cells, which are also stained by this mAb. (B) Wild type. FB, SB, and T are indicated. (C) An ISN from a *Dlar* embryo, displaying the SB+ phenotype. (D) An ISN from a *Dlar; Ptp69D* embryo, displaying the SB phenotype. (E) An ISN from a *Dlar; Ptp69D; Ptp99A* embryo, displaying the FB phenotype. (F–N) Bar graphs showing the ISN phenotypes of different mutant combinations. The ordinates represent the penetrances (in % of hemisegments) of the various phenotypes. The T phenotype (axons reach the terminal arbor position; dark blue bars) and SB+ phenotype (axons stall between SB and T; light blue bars) categories are combined into one column labeled 2+, meaning that these ISNs extend beyond SB. SB (stop at second branch point) phenotype: purple bars. FB (stop at first branch point) phenotype: red bars. *n* values: F, 101; G, 107; H, 118; I, 83; J, 256; K, 96; L, 215; M, 105; N, 118.

the RP axons sometimes extend on only one side of the embryo (Fig. 2D, missing pathway indicated by bracket). mAb 22C10 also stains the VUM axons, which originate at the midline, grow anteriorly, and then bifurcate. In quadruple RNAi embryos, the VUM axons often fail to bifurcate, so that a VUM pathway is observed only on one side (data not shown). Other early axons stained by the 1D4 and 22C10 mAbs, such as those of the aCC, RP2, and U motor neurons, usually develop normally in quadruple RNAi embryos.

By stages 15–16, a continuous, straight longitudinal 22C10-positive pathway has developed (Fig. 2C, dotted lines). This is missing in quadruple RNAi embryos (Fig. 2D). 22C10 also stains the axons of peripheral sensory neurons, which begin to enter the CNS by this time, following the ISN and SN root motor pathways (Fig.

2C). These combined motor/sensory nerves appear relatively normal in quadruple RNAi embryos (Fig. 2D), except in segments in which the RP axons fail to pioneer a section of the ISN pathway (bracket).

DPTP10D Regulates Outgrowth and Bifurcation of the SNa Motor Nerve

DPTP10D is apparently expressed at higher levels on SNa axons and growth cones than on other motor pathways. Figure 3 shows staining of the SNa by anti-DPTP10D during its outgrowth (stage 15); DPTP10D expression on other motor nerves at this time is apparently below the limit of detection. It is usually not possible to visualize staining of individual motor nerves, which contain only a few axons, with antibodies against the RPTPs. Staining of the thicker ISN and SN roots as they leave the CNS can be observed, however (Desai *et al.*, 1994; Tian *et al.*, 1991), suggesting that all of the RPTPs are in fact expressed on both ISN and SN motor pathways. In embryos with six copies of the wild-type *Ptp69D* gene, all individual motor nerves can be clearly visualized with anti-DPTP69D mAbs (Desai *et al.*, 1996). Finally, *in situ* hybridization analysis indicates that DPTP10D and DPTP99A mRNAs are expressed by identified motor neurons (Yang *et al.*, 1991).

The SNa nerve has a characteristic bifurcated morphology. The bifurcation occurs at a choice point located between muscles 22 and 23. The posterior (or lateral) branch of the SNa innervates muscles 5 and 8, and the anterior (or dorsal) branch innervates muscles 21–24 (Figs. 4A and 4B; the N (normal) SNa phenotype is indicated by the green bars). SNa development is unaffected in all single *Rptp* mutants.

In *Ptp10D; Ptp69D* double-mutant embryos, an SNa bifurcation is not observed in >40% of hemisegments. The mutant SNa nerves either stall at the bifurcation point or, more commonly, have only one branch (either anterior or posterior) extending beyond this point (Figs. 4C and 4F; the failure-to-bifurcate (B) phenotype is indicated by the purple bars). Note that this phenotype could be due either to both sets of SNa axons (the 5 and 8 and 21–24 axons) following one pathway after the normal bifurcation point or to a failure of one set of axons to grow out past the bifurcation point. This cannot be determined at present since there are no markers that distinguish between these two sets of axons.

Analysis of all double-, triple-, and quadruple-mutant phenotypes shows that SNa bifurcation exhibits a complex dependence on RPTP function. Bifurcation failures (B phenotype) are observed at a lower frequency (25%) in another double-mutant genotype, *Dlar; Ptp69D* (Fig. 4G), but are never seen in *Ptp10D; Dlar* (data not shown). Removing either of the two remaining RPTPs from *Ptp10D; Dlar*, however, now causes 46–58% of SNa nerves to fail to bifurcate (Figs. 4H and 4I). These data indicate that all four of the RPTPs participate in SNa bifurcation and/or outgrowth past the bifurcation point (see Discussion).

All four RPTPs are also involved in facilitation of SNa outgrowth to the bifurcation point. In quadruple-mutant embryos, 55% of SNa nerves either do not reach the bifurcation point at all or are very thin and wandering (Figs. 4D, 4E, and 4L; this is denoted as the "short/thin" (ST) phenotype and is indicated by red bars). These phenotypes suggest that some SNa axons may not enter the nerve at all and that the remaining axons are impaired in their outgrowth.

Defective SNa outgrowth (ST phenotype) is not observed in any double mutant and is also very rare in any triple mutant in which *Dlar* or *Ptp69D* is wild-type (Figs. 4G and 4H). If *Dlar* and *Ptp69D* are both mutant, removal of DPTP99A or DPTP10D results in defective outgrowth of about 40% of SNa nerves, and removal of both produces the 55% penetrance seen in the quadruple mutant (Figs. 4J–4L). Thus, expression of DLAR alone, DPTP69D alone, or DPTP10D *plus* DPTP99A is sufficient to allow normal outgrowth of SNa axons to the bifurcation point in >95% of hemisegments.

Loss of DPTP10D Function Partially Suppresses the ISN Truncation Phenotypes of Dlar; Ptp69D; Ptp99A Triple Mutants

The ISN passes two major lateral branch points, denoted FB and SB, before reaching the position of its terminal arbor (T) at the proximal edge of muscle 1 (Figs. 5A and 5B). DLAR is central to ISN guidance or outgrowth, because ISN truncations are seldom observed in any genotype in which *Dlar* is wild type. In *Dlar; Ptp69D* double mutants, about 50% of ISNs terminate at the SB position (Figs. 5D and 5F; this SB phenotype is indicated by purple bars). The remainder of the ISNs either terminate between SB and T (SB+ phenotype; Fig. 5C) or make an abnormally small terminal arbor. The T phenotype is defined as that in which axons reach the normal terminal arbor position. Phenotypes in which axons pass SB (SB+ and T) are combined into the bicolored light/dark blue bars, which are labeled 2+. In *Dlar; Ptp69D; Ptp99A* triple mutants, about 50% of ISNs terminate at the FB position (Figs. 5E and 5H; this FB phenotype is indicated by red bars), and most of the remainder stop at SB (Desai *et al.*, 1997).

To examine the role of DPTP10D in development of

the ISN pathway, we analyzed the phenotypes of *Ptp10D* mutations combined with the other *Rptp* mutations in double, triple, and quadruple mutant combinations. Our analysis shows that the absence of DPTP10D function does not adversely affect ISN guidance, because the phenotypes of *Rptp* mutant combinations are not significantly strengthened by removing DPTP10D. First, multiply-mutant genotypes that do not include mutant *Dlar* have weak ISN phenotypes whether or not *Ptp10D* is mutant. For example, <10% of ISNs prematurely terminate (3% SB, 6% SB+) in *Ptp10D; Ptp69D; Ptp99A* triple mutants (Fig. 5N). Second, the phenotypes of embryos in which *Dlar* is mutant are not worsened by inclusion of mutant *Ptp10D*. For example, 75% of ISNs prematurely terminate in *Dlar; Ptp69D* (27% SB+, 45% SB) and 78% in *Ptp10D; Dlar; Ptp69D* (38% SB+, 38% SB; Figs. 5F and 5G). Sixty-five percent of ISNs prematurely terminate in *Dlar; Ptp99A* (39% SB+, 21% SB) and 52% in *Ptp10D; Dlar; Ptp99A* (30% SB+, 21% SB; Figs. 5L and 5M).

DPTP10D actually functions in opposition to the other RPTPs in regulating ISN outgrowth past the FB and SB branch points. This is shown most clearly by a comparison of the phenotypes of *Dlar; Ptp69D; Ptp99A* triple mutants and *Ptp10D; Dlar; Ptp69D; Ptp99A* quadruple mutants. In the triple-mutant embryos, 52% of ISNs stop at FB, 37% stop at SB, and only 11% grow past SB. In quadruple mutants, however, only 15% of ISNs stop at FB, 53% stop at SB, and 31% extend beyond SB (Figs. 5H and 5I). Thus, the distribution of ISN lengths is shifted toward wild type by removal of DPTP10D function from a triple mutant. This result is formally similar to, but less dramatic than, our earlier finding that removal of DPTP99A function suppresses the ISNb parallel-bypass phenotype of *Dlar* (31% partial or complete parallel bypass in *Dlar* vs 1% in *Dlar; Ptp99A;* Desai *et al.*, 1997).

DPTP10D Acts Together with the Other Three RPTPs to Facilitate ISNb Defasciculation at the Exit Junction

The axons of the ISNb (SNb) nerve innervate the VLMs. ISNb growth cones extend out the ISN root and defasciculate from the common ISN pathway at the exit junction (Figs. 6A, 6F, and 6G). ISNd (SNd) axons also leave the ISN at the exit junction and follow the pathway laid down by the earlier ISNb axons until they reach a nearby second junction where ISNd separates from ISNb (Figs. 6A and 6G). In *Dlar* embryos (and in all mutant combinations in which *Dlar* is mutant), ISNd is usually missing (Krueger *et al.*, 1996). Since they cannot be visualized separately from ISN and ISNb axons (no markers distinguish these axons), it is unknown whether mutant ISNd axons follow one of the other ISN branches or fail to even reach the exit junction. Near the point at which ISNd and ISNb separate, ISNb enters the VLM field. The green bars in the figure, labeled N, indicate the percentage of hemisegments in which the ISNb nerve is able to grow into the muscle field.

Our previous results showed that DLAR, DPTP69D, and DPTP99A are all involved in ISNb navigation at the exit junction (Desai *et al.*, 1997). In triple-mutant embryos lacking all three of these RPTPs, about 30% of ISNb nerves fail to leave the ISN at the exit junction and continue to grow out along the common ISN pathway (bypass phenotype). In most of these bypass hemisegments, only one ISN branch is visible, and it is usually thicker than normal (Figs. 6B and 6H). In a side view of these hemisegments (like that diagrammed in Fig. 6F), a single nerve growing exclusively on the external side of the VLMs would be observed. (This is the side farthest from the lens, since the dissected embryos are viewed from the internal side.) We interpret this "fusion bypass" (FBP) phenotype as indicating that the ISNb nerve grew out along the common ISN pathway. It is also possible that some ISNb axons in bypass hemisegments fail to extend past the entrance to the VLM field; but most are likely to continue to grow along the ISN, because the ISN is thicker in such hemisegments.

In quadruple-mutant embryos, no axons are ever observed to enter the VLM field. The frequency of bypass phenotypes is increased to 76%, indicating that DPTP10D also contributes to the decision of ISNb axons to leave the ISN at the exit junction (Fig. 6P). We note that in some triple- and quadruple-mutant hemisegments (17% in the quadruple mutant collection; Fig. 6P) a small gap between the ISN and the ISNb bundles is visible at the exit junction, but the bundles fuse together again after a short distance. We think that these also represent failures of the ISNb to leave correctly at the exit junction, because the axons return to the ISN without growing past the VLMs. However, we lack a clear quantitative way to separate these phenotypes from the "parallel bypass" (PBP) phenotype seen in *Dlar* embryos, in which the ISNb nerve grows out past the VLMs as a separate pathway before returning to the ISN (Krueger *et al.*, 1996, Desai *et al.*, 1997; see diagram in Fig. 6J). Because of this, we have classified these "gapped" triple- and quadruple-mutant phenotypes as PBP and have grouped the FBP (gold) and PBP (red) phenotypes together into the bicolored red/gold bars labeled BP (bypass). The heights of these bicolored bars

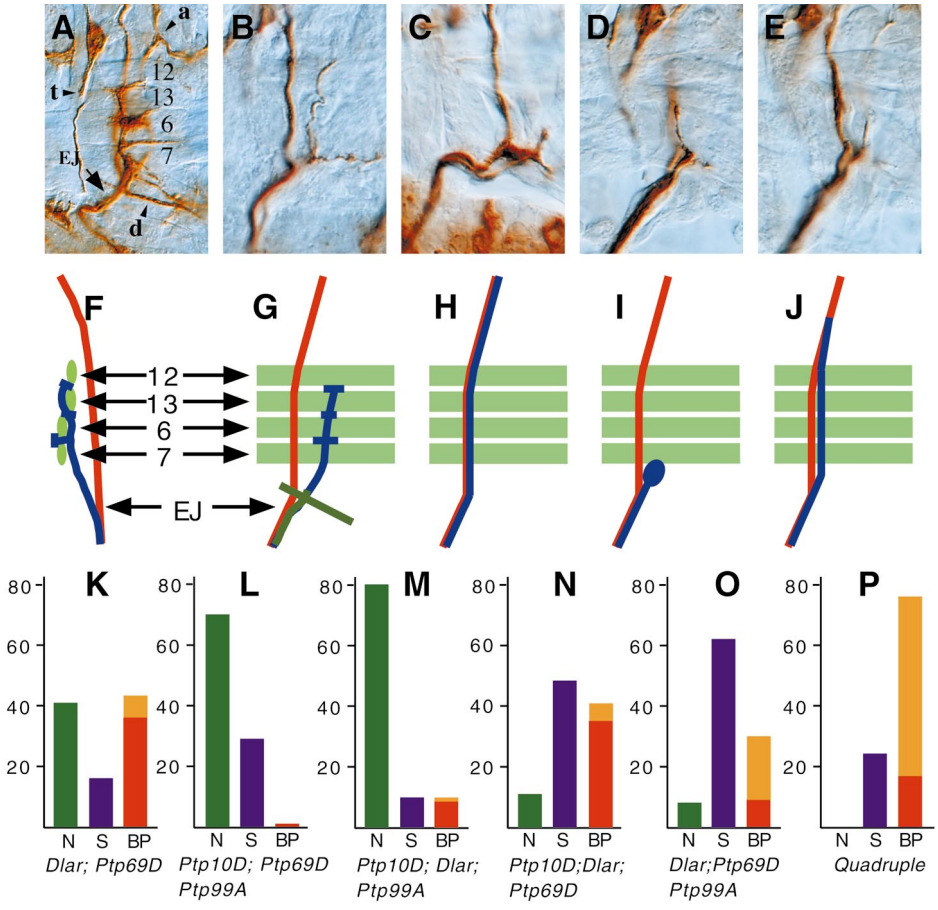

FIG. 6. ISNb phenotypes in *Rptp* mutant embryos. (A) Wild-type late stage 16/early stage 17 ISNb stained with mAb 1D4. Four of the ISNb target muscles (6, 7, 12, 13), the SNa bifurcation point (a), the ISNd (d), the transverse nerve (t), and the exit junction (EJ) are labeled. The ISN is out of focus underneath the muscles. (B–E) Each image shows an ISNb from a late stage 16/early stage 17 quadruple-mutant embryo stained with mAb 1D4. (B) Fusion bypass: the ISNb is completely fused with the ISN, which has become thicker. The thin branches to its right are SNa and SNc. (C) The ISNb stalls immediately after exiting the ISN. (D, E) Two different focal planes of a quadruple-mutant ISNb. (D) is at the focal plane of the VLMs and shows a small branch on the wrong (internal) face of muscles 6/7. The 6/7 synapse extends to the internal face of muscles 6/7, but the nerve trajectory is on the external face. (E) is a deeper focal plane, showing that the rest of the ISNb has probably fused with the ISN. (F–J) Schematic diagrams. The ISNb is blue, the ISN is red, the ISNd is light green, and the muscles are aqua. (F, G) Wild type, side (internal to left) and top views. (H) Fusion bypass. (I) Stall. (J) Parallel bypass, as in *Dlar*. (K–P) Bar graphs showing the ISN phenotypes of different mutant combinations. The ordinates represent the penetrances (in % of hemisegments) of the various phenotypes. N (green bars): the ISNb enters the VLM field. Note that these ISNb nerves are not necessarily wild type; in these genotypes most of them would make further pathfinding errors among the muscle fibers. Here, however, we are only scoring whether or not the ISNb grows into the VLM field. Stall (S) phenotype: purple bars. Bypass (BP) phenotypes: bicolored red/gold bars. Fusion bypass is indicated by the gold portion of the bars and parallel bypass by the red portion. *n* values: K, 119; L, 119; M, 108; N, 106; O, 119; P, 76.

thus represent the total frequency of bypass phenotypes.

In the remaining 24% of quadruple-mutant hemisegments, the ISNb nerve appears to leave the ISN but immediately stalls (Figs. 6C and 6I) or extends short abnormal branches (Figs. 6D and 6E). We have classified all such hemisegments as stall (S) phenotypes (indicated by purple bars). Figures 6D and 6E show two focal planes of a hemisegment in which a small branch grew out on the wrong (internal) face of muscles 6 and 7. Normally the ISNb remains on the external face of the VLMs until it reaches muscle 13; only the final ISNb projection to muscle 12 grows on the internal face (see Fig. 6F).

In summary, our analysis indicates that DPTP10D has a role in facilitating ISNb defasciculation from the common ISN pathway and may also help these axons enter the VLM field (see Discussion). Examination of

single-, double-, and triple-mutant phenotypes suggests that DPTP10D does not contribute strongly to the later decisions (navigation among the VLMs and synaptogenesis) made by ISNb axons after entering the VLM field. This is demonstrated by the fact that the percentage of abnormal branches within the muscle field in an *Rptp* genotype is the same whether or not DPTP10D is also removed from that genotype. For example, the penetrances of branching phenotypes within the VLMs in *Ptp69D* and *Ptp10D; Ptp69D* are the same (data not shown).

DISCUSSION

Genetic studies of three *Drosophila* neural RPTPs (DLAR, DPTP69D, and DPTP99A) have shown that these transmembrane receptors are important components of the mechanisms that regulate the formation of specific synaptic connections in the neuromuscular system and the optic lobes (Desai *et al.*, 1996, 1997; Krueger *et al.*, 1996; Garrity *et al.*, 1999; Wills *et al.*, 1999). The fourth neural RPTP, DPTP10D, was shown to function together with DPTP69D in regulating repulsion of axons from the midline of the CNS (Sun *et al.*, 2000). In this paper, we analyze the roles of DPTP10D and the other three neural RPTPs in controlling axon guidance, studying the phenotypes of double, triple, and quadruple *Rptp* mutant combinations. Our results provide insights into how the four RPTPs work together and in opposition to each other in controlling specific growth-cone pathfinding decisions within the embryonic neuromuscular system and the CNS.

The RPTPs have partially redundant (overlapping) activities in controlling most axon guidance decisions in the neuromuscular system. For example, extension of the ISN past the first lateral branch point, FB, can be facilitated by DLAR, DPTP69D, or DPTP99A (Desai *et al.*, 1997). The failure to grow out past FB in this triple mutant could be due to an error in guidance, so that the growth cones fail to recognize the next intermediate target. Alternatively, the ISN axons might develop an impairment in their ability to grow that causes them to stall at this specific point.

In other cases, two RPTPs have "collaborative" relationships. Outgrowth of the SNa nerve to its bifurcation point, or of the ISNb nerve to the muscle entry site, can be facilitated by DLAR or DPTP69D, but not by DPTP10D or DPTP99A alone. DPTP10D *plus* DPTP99A can allow normal outgrowth, however (Figs. 4 and 6; see below). Finally, for some decisions the RPTPs display antagonistic or competitive interactions. Entry of the ISNb into the VLM field is regulated by competition between DLAR and DPTP99A (Desai *et al.*, 1997), while DPTP10D has an antagonistic relationship with the other RPTPs in controlling ISN extension past lateral branch points (Fig. 5).

To describe more clearly how DPTP10D and the other RPTPs control motor axon guidance decisions, we now employ a different format in which, rather than discussing the penetrance of the defects produced by combinations of mutations, we begin by asking what percentage of motor nerves have appropriate trajectories past their first presumed choice point in a quadruple mutant lacking all of the known neural RPTPs. We then genetically "add back" each RPTP and calculate what percentage of the nerves now follow the correct trajectory. For subsequent choice points along a pathway, we consider only the subpopulation of mutant nerves that followed a normal pathway past the previous choice point and then ask how adding back RPTPs influences their ability to navigate correctly at the next choice point. "Flow charts" of this process are shown in Fig. 7.

For SNa guidance, the flow chart reveals that outgrowth to the bifurcation point can be completely restored by adding DLAR or DPTP69D to the quadruple mutant (45% correct → 95%), but only partially restored by DPTP10D or DPTP99A (to 60%; Fig. 7A). Addition of *both* DPTP10D and DPTP99A restores extension to >95%, however.

Bifurcation of the SNa into its anterior and posterior branches almost never occurs in a quadruple mutant (1%); it can be partially restored by DLAR or DPTP69D (to 53%), but DPTP10D is less effective (20%) and DPTP99A is ineffective (7%). DPTP99A also cannot restore bifurcation when added to triple mutants expressing only DLAR (53% → 57%). However, DPTP99A is quite effective when added to triple mutants expressing only DPTP10D (20% → 75%) or only DPTP69D (53% → 96%; Fig. 7B). These results suggest a collaborative relationship at this decision point between DPTP99A and DPTP10D and, to a lesser extent, between DPTP99A and DPTP69D. DPTP99A cannot facilitate SNa bifurcation when expressed in the absence of DPTP69D and DPTP10D, but if one of these other RPTPs is expressed, DPTP99A can now collaborate with it to allow the nerve to bifurcate normally.

We now discuss progression of the ISN past the FB and SB branch points. In a quadruple mutant, 84% of ISNs extend past FB. Adding back DLAR, DPTP69D, or DPTP99A increases this percentage to >95%, but adding back DPTP10D *decreases* the percentage of extension past FB to 48%. Adding any one of the other three RPTPs to the triple mutant that expresses only

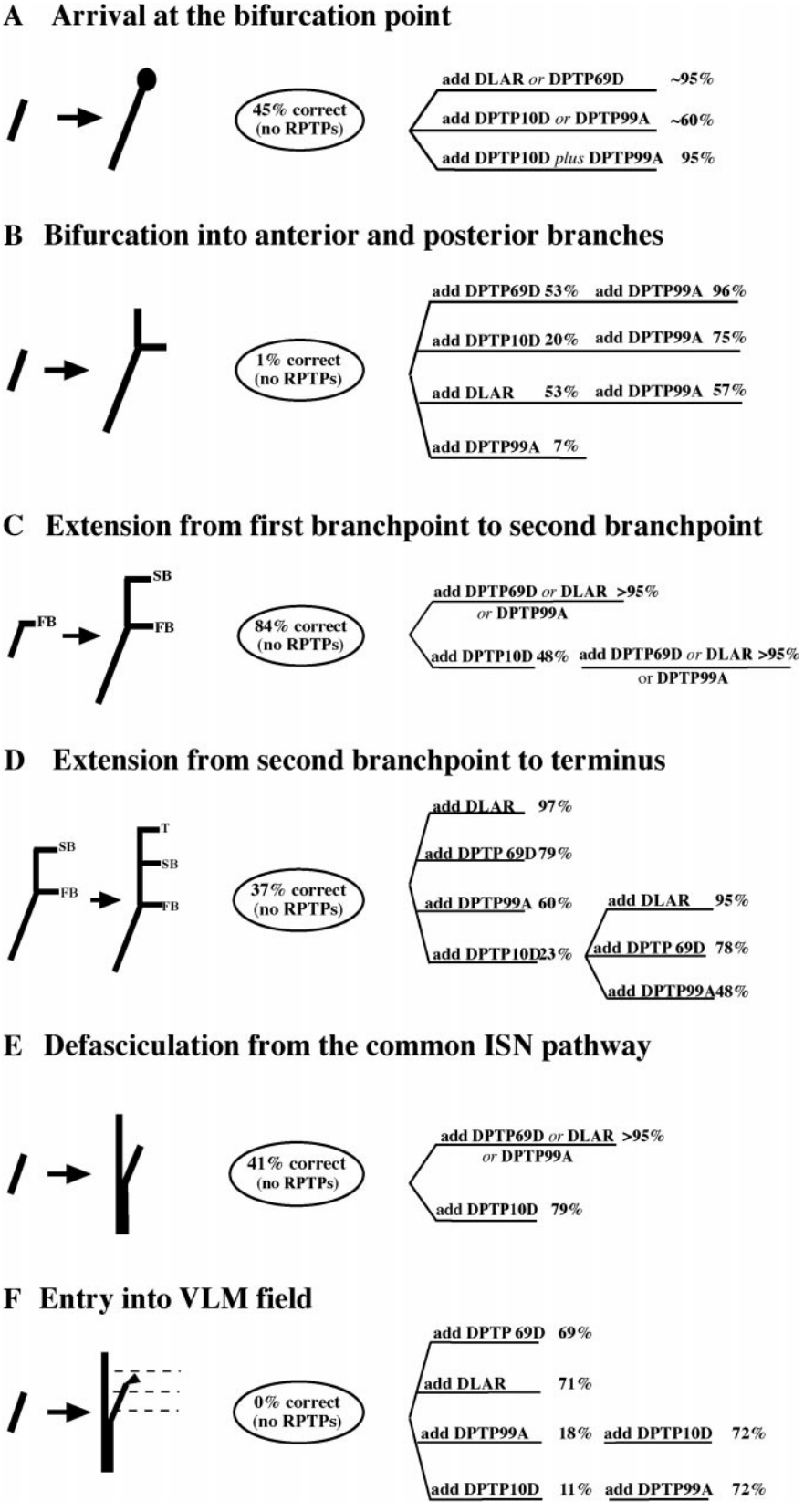

FIG. 7. Flow charts of motor axon phenotypes, showing how each RPTP contributes to six different axon guidance decisions. The frequency (in %) with which the correct pathway choice is made by a motor nerve in quadruple mutants is indicated on the left, and the frequencies of correct choices after genetically adding back the indicated RPTPs are to the right.

DPTP10D now restores the ability to extend past FB in >95% of cases (Fig. 7C).

For progression past SB, DLAR, DPTP69D, and DPTP99A now differ in their abilities to facilitate the correct decision. DLAR completely rescues (from 37 to >95%), while DPTP99A is relatively ineffective (to 60%) and DPTP69D is intermediate (79%). Again, adding DPTP10D *decreases* the percentage of successful extension past SB (from 37 to 23%; Fig. 7D). When DLAR, DPTP69D, or DPTP99A is added to the triple mutant in which only DPTP10D is expressed, their relative effectiveness at restoring growth past SB is the same as for addition to the quadruple mutant.

These data suggest a competitive relationship between DPTP10D and the other RPTPs. In the *Dlar; Ptp69D; Ptp99A* triple mutant, there is excess DPTP10D activity (in a formal genetic sense), and this favors truncation at FB or SB. When DPTP10D is removed, the percentage of successful extension is increased at both branch points.

ISNb defasciculation from the common ISN pathway at the exit junction can be facilitated by expression of any of the four RPTPs, but DPTP69D, DLAR, and DPTP99A are more effective than DPTP10D (41% → >95% for the first three vs 41% → 79% for DPTP10D; Fig. 7E). Extension of the ISNb from the exit junction to the muscle entry site is more complex. ISNd axons normally separate from the ISNb shortly after it leaves the ISN, but it is likely that these axons are not yet present during the time at which ISNb is pioneering this section of its pathway. Thus, the ISNb "stall" phenotype is probably produced by a failure of ISNb extension rather than by a failure to separate from ISNd axons. A further piece of evidence supporting this conclusion is that ISNd fails to separate from ISNb (or does not extend at all) in *Dlar* single mutants (Krueger *et al.*, 1996), but ISNb does not stall in this genotype (Desai *et al.*, 1997).

The ISNb never successfully enters the VLMs in quadruple mutants (that is, all quadruple mutant ISNbs that manage to defasciculate from the ISN stall before the muscle entry site). DPTP69D, and to a lesser extent DLAR, can restore successful entry into the muscle field (0% → 89 and 71%, respectively). DPTP10D and DPTP99A, however, are quite ineffective (0% → 11 and 18%, respectively). Interestingly, however, when *one* of this pair of RPTPs is present, addition of the other can now effectively restore extension (11 or 18% → 72%; Fig. 7F). These results, like those described above for SNa, suggest a collaborative relationship between DPTP10D and DPTP99A in which the two RPTPs can function only as a pair at this decision point.

Finally, we can also construct a qualitative flow chart for CNS axon guidance, although we cannot describe guidance along the longitudinal pathways in a quantitative manner because individual hemisegments cannot be considered independently. Many interneuronal axons traverse several segments, so that phenotypes in different segments influence each other (Schmid *et al.*, 1999).

In the absence of all four neural RPTPs, most 1D4-positive longitudinal pathways appear to become commissural and cross the midline (Fig. 1). Examination of earlier embryos shows that the descending MP1 longitudinal pioneer pathway is rerouted across the midline when all four RPTPs are missing (Fig. 2). This phenotype is also seen in *robo* mutants (Kidd *et al.*, 1998a,b).

Adding back only DPTP10D or only DPTP69D to the quadruple mutant restores an almost wild-type 1D4 pattern. The resulting *Dlar; Ptp69D; Ptp99A* and *Ptp10D; Dlar; Ptp99A* triple mutants differ from wild type primarily in that the outer 1D4-positive longitudinal bundle is discontinuous (Fig. 1). Thus, these two RPTPs are central to control of guidance of CNS axons across the midline.

In contrast, adding back DPTP99A to a quadruple mutant has a much less dramatic effect. Some longitudinal bundles are present in *Ptp10D; Dlar; Ptp69D* triple mutants, but many 1D4-positive axons still cross the midline, and these often do not respect the normal borders of the commissural tracts. Adding back DLAR to the *Ptp10D; Dlar; Ptp69D* triple mutant produces a more regular pattern, in which the crossing 1D4-positive axons remain with the normal boundaries of the commissural tracts. Finally, adding back DPTP10D or DPTP69D to the *Ptp10D; Ptp69D* double mutant to create a single mutant restores the CNS to a completely wild-type morphology, in which there are three distinct longitudinal bundles and no 1D4-positive axons crossing the midline.

The molecular mechanisms involved in these three types of relationships (partially redundant, collaborative, and competitive) among the RPTPs are unknown. We also do not know why each of the individual RPTPs regulates only a specific subset of outgrowth and guidance decisions, since they appear to be expressed on every motor axon. It is attractive to speculate that RPTP enzymatic activity and/or localization within growth cones is regulated by engagement of RPTP ligands localized to specific cells along the pathways of the motor nerves.

The nature of these putative ligands is unknown. Indeed, *in vivo* ligands for RPTPs have not been identified in any system. Some vertebrate and leech RPTPs

can function as homophilic adhesion molecules (Baker *et al.*, 2000; Brady-Kalnay *et al.*, 1993; Cheng *et al.*, 1997; Wang and Bixby, 1999; Zondag *et al.*, 1995). We have not been able to observe homophilic adhesion activity for the *Drosophila* RPTPs, however. RPTPs can also interact heterophilically with ligands *in vitro.* RPTPβ/ζ binds to the secreted cytokines pleiotrophin and midkine and to the neural adhesion molecules contactin and F3 (Maeda *et al.*, 1996, 1999; Peles *et al.*, 1995; Revest *et al.*, 1999). LAR can interact with a laminin–nidogen complex (O'Grady *et al.*, 1998). Chicken CRYPα extracellular domains bind to specific areas of the retinotectal system, suggesting that ligands are located there. These have not been molecularly identified, however (Haj *et al.*, 1999).

The rescue data presented here (Table 1) and in Garrity *et al.* (1999) suggest that interaction with extracellular proteins is required for DPTP69D function. Mutants in which the FN3 repeats of the extracellular domain are deleted, or constructs in which the extracellular domain is replaced with mammalian RPTPμ sequences, do not rescue the *Ptp10D; Ptp69D* CNS axon guidance phenotype. FN3 repeat deletions also do not rescue the *Ptp69D* photoreceptor axon guidance phenotype in third-instar larvae (Garrity *et al.*, 1999). The Ig domains are not required for phenotypic rescue, but are necessary for viability, suggesting that they function in other pathways. These results suggest that interaction of the FN3 repeats with other proteins is necessary for guidance. These could be ligands on other cells or coreceptors on the DPTP69D-expressing cell.

Like most other RPTPs, DPTP69D and DLAR each have two cytoplasmic PTP domains, D1 and D2, that are potentially active as phosphatases. D2 domains, however, are sometimes catalytically inactive and always display less catalytic activity than D1 domains, at least *in vitro* (see Nam *et al.*, 1999, for a discussion of this point). DPTP99A-D2 lacks the essential cysteine residue, indicating that it cannot be catalytically active, and DPTP10D has only a single PTP domain. Enzymatic activity is likely to be required for DPTP69D function during axon guidance decisions, because mutants in which both PTP domains are inactivated by point mutations fail to rescue axon guidance phenotypes (Garrity *et al.*, 1999; Table 1). The two domains apparently have redundant functions in R1–6 photoreceptor or embryonic CNS axon guidance, since mutants in which only one domain is inactivated (D1) or deleted (D2) still rescue. These single PTP domain mutants do not rescue viability, however, indicating that the two domains have distinct functions in other pathways. We note that Newsome *et al.* (2000) found a point mutation in D1 that confers the photoreceptor guidance defect; they did not determine, however, whether the mutant DPTP69D is still expressed. If mutant protein is unstable, these results would not be in conflict with the Garrity *et al.* (1999) rescue experiments.

One mechanism that could explain both collaboration and competition among the RPTPs is ligand-driven formation of hetero-oligomers. For example, if a DPTP10D/DPTP99A hetero-oligomer could signal at a specific choice point (where a particular oligomerizing ligand might be present) but DPTP10D and DPTP99A monomers were inactive in that context, one could explain the apparent collaborative role for DPTP10D *plus* DPTP99A in facilitating guidance and/or extension at this choice point. Conversely, competition could be mediated by formation of inactive RPTP hetero-oligomers from active monomers. For example, DLAR might suppress DPTP99A activity at the muscle entry site by forming a hetero-oligomer with it in which DPTP99A was inactive (Desai *et al.*, 1997).

The existence of inactive RPTP dimers has been demonstrated for mammalian RPTPα. In its crystal structure, a conserved helical region (the "wedge") between the membrane and PTP-D1 inserts into the active site of the other D1 domain in the dimer. This structure predicts that the RPTPα dimer would be catalytically inactive because the wedge would occlude access to the active site (Bilwes *et al.*, 1996). Wedge-mediated inactivation of RPTPα catalytic activity has been directly demonstrated by forced dimerization of mutants expressed in transfected cells (Jiang *et al.*, 1999, 2000). Consistent with this model for RPTP regulation, introduction of wedge mutations into an EGF receptor (extracellular)–CD45 RPTP (intracellular) chimera blocks inhibition of CD45 signaling caused by EGF-mediated homodimerization (Majeti *et al.*, 1998). Finally, pleiotrophin binding to RPTPβ/ζ reduces its catalytic activity, possibly through ligand-induced dimerization (Meng *et al.*, 2000). It is unknown whether this effect on phosphatase activity requires the wedge region.

Wedge-mediated dimerization, however, is only one of many potential interactions that occur among RPTP cytoplasmic domains, and we have no evidence that it is important *in vivo.* In fact, the wedge may be dispensable for DPTP69D function in axon guidance, since wedge mutants fully rescue the optic lobe and embryonic CNS phenotypes (Garrity *et al.*, 1999, Table 1; these mutants rescue lethality only poorly, however, suggesting that the wedge does have a function during development). It is also unclear whether other RPTPs can even form this type of dimer. The crystal structures of LAR and RPTPμ do not display wedge–D1 interactions,

and such an interaction might be precluded for LAR because of intramolecular contacts between LAR D1 and D2 (Hoffmann *et al.*, 1997). Biochemical studies indicate that the D2 domains of RPTPα, LAR, CD45, and other RPTPs can bind to a variety of D1 domains, and also to the wedge region, either intramolecularly or intermolecularly (Blanchetot and den Hertog, 2000; Felberg and Johnson, 1998; Nam *et al.*, 1999; Wallace *et al.*, 1998). These interactions can inhibit or increase enzymatic activity. Elucidation of the biochemical mechanisms that underlie the genetic relationships among the *Drosophila* RPTPs is likely to require identification of the ligands, coreceptors, and substrates that they recognize *in vivo.*

EXPERIMENTAL METHODS

Genetics and Immunohistochemistry

To eliminate DPTP10D expression, we used the null allele *Ptp10D*^{1}, which is homozygous/hemizygous viable and fertile and affects only DPTP10D (Sun *et al.*, 2000). *Ptp10D*^{1} was generated from the P element insertion *EP(X)1172* (Rorth *et al.*, 1998). Analysis of the complete genome sequence shows that *EP(X)1172* is immediately upstream of *Ptp10D,* but distant from other predicted genes, and that the *Ptp10D*^{1} deletion cleanly removes the first exon of *Ptp10D* without approaching other predicted genes (see map in Sun *et al.*, 2000). Two other independently generated *Ptp10D* alleles, *Df(1)59* and *Df(1)101,* produce the same phenotypes as *Ptp10D*^{1} when combined with *Ptp69D* (Sun *et al.*, 2000); we did not use these alleles in the present study because they also affect the neighboring gene 3′ to *Ptp10D, bifocal.* For the other three *Rptp* genes, we used null transheterozygous combinations of alleles that were employed by Desai *et al.* (1997), in order to be able to directly compare results on phenotypic penetrances. For *Ptp69D,* we used *Ptp69D*^{1}/*Df(3L)8ex25* (Desai *et al.*, 1996). For *Dlar, Dlar*$^{5.5}$/*Dlar*$^{13.2}$ was used (Krueger *et al.*, 1996). For *Ptp99A, Ptp99A*^{1}/*Df(3R)R3* was used (Hamilton *et al.*, 1995). For transgenic rescue experiments, the GAL4-driven DPTP69D mutant transgene lines described by Garrity *et al.* (1999) were used. These transgenes and *Elav-GAL4* drivers were introduced into *Ptp10D; Ptp69D* mutant backgrounds using standard genetic methods. We also used a transgene, not described in Garrity *et al.* (1999), in which the entire extracellular domain of DPTP69D is replaced by the extracellular domain of mammalian RPTPμ (kindly provided by P. Garrity, C.-H. Lee, and L. Zipursky). Late stage 16/early stage 17 embryos were collected from crosses between heterozygous flies bearing various combinations of mutant alleles and/or transgenes. The desired mutant embryos were identified based on the absence of staining with mAbs specific for each RPTP and/or by the absence of staining with anti-β-galactosidase mAb (Promega), which detects the presence of the *lacZ* gene on the balancer chromosomes. The anti-RPTP mAbs used were 45E10 (DPTP10D; Tian *et al.*, 1991), 3A6 (DPTP99A; Tian *et al.*, 1991), 3F11 (DPTP69D; Desai *et al.*, 1994), and 8C4 (DLAR; B. Burkemper and K.Z., unpublished). The mutant embryos were then restained with mAb 1D4 (Van Vactor *et al.*, 1993) to reveal motor axon and CNS pathways, dissected, and photographed on a Zeiss Axioplan microscope using Nomarski optics. All mAb supernatants were used at 1:5 to 1:10 dilutions. Whole-mount antibody staining of fly embryos using horseradish peroxidase immunohistochemistry was performed as described (Patel, 1994).

RNAi Experiments

Wild-type embryos were collected at stage 5, hand dechorionated, mounted on coverslips, and desiccated for 6 min at 18°C. They were then covered with 650 cS halocarbon oil and injected with <1 μM solutions of dsRNA in injection buffer (Kennerdell and Carthew, 1998), using a Nikon inverted Diaphot microscope with a 100× Nikon Planapo oil immersion lens. Embryos were viewed with a Hamamatsu CCD camera and a Sony video monitor and injected with the aid of Leitz micromanipulators. Details of plasmids used for dsRNA synthesis are available on request; RPTP dsRNAs were between 900 and 1.6 kb in length. Transcription and annealing were done as described by Kennerdell and Carthew (1998). When combinations of RNA were injected, summed concentrations of constituent RNAs were never greater than 1 μM. After injection, embryos were left at 18°C for 30 h. They were then filleted, fixed in 5% paraformaldehyde, and stained with mAbs 22C10 or 1D4 as described above. Embryos were viewed on a Zeiss Axioplan microscope with a 63× oil immersion lens and were photographed using an Olympus Magnafire digital camera system.

ACKNOWLEDGMENTS

We thank Bruce Burkemper for the anti-DLAR mAb 8C4; Chand Desai for ISN and ISNb images and discussions on motor axon phenotypes; Paul Garrity, Chi-Hon Lee, and Larry Zipursky for the DPTP69D transgenic rescue lines; and Tony Hunter for discussions on

RPTP dimerization. This work was supported by an NIH RO1 grant (NS28182) and a Human Frontiers Science Project grant (RG0122/1997-B) to K.Z.

REFERENCES

Adams, M. D., Celniker, S. E., Holt, R. A., Evans, C. A., Gocayne, J. D., Amanatides, P. G., Scherer, S. E., Li, P. W., Hoskins, R. A., Galle, R. F., *et al.* (2000). The genome sequence of Drosophila melanogaster. *Science* **287:** 2185–2195.

Baker, M. W., Rauth, S. J., and Macagno, E. R. (2000). Possible role of the receptor protein tyrosine phosphatase HmLAR2 in interbranch repulsion in a leech embryonic cell. *J. Neurobiol.* **45:** 47–60.

Bilwes, A. M., Den Hertog, J., Hunter, T., and Noel, J. P. (1996). Structural basis for inhibition of receptor protein tyrosine phosphatase-alpha by dimerization. *Nature* **382:** 555–559.

Blanchetot, C., and den Hertog, J. (2000). Multiple interactions between receptor protein-tyrosine phosphatase (RPTP) alpha and membrane-distal protein-tyrosine phosphatase domains of various RPTPs. *J. Biol. Chem.* **275:** 12446–12452.

Brady-Kalnay, S. M., Flint, A. J., and Tonks, N. K. (1993). Homophilic binding of PTPμ, a receptor-type protein tyrosine phosphatase, can mediate cell–cell aggregation. *J. Cell Biol.* **122:** 961–972.

Brand, A. H., and Perrimon, N. (1993). Targeted gene expression as a means of altering cell fates and generating dominant phenotypes. *Development* **118:** 401–414.

Cheng, J., Wu, K., Armanini, M., Orourke, N., Dowbenko, D., and Lasky, L. A. (1997). A novel protein-tyrosine phosphatase related to the homotypically adhering kappa and mu receptors. *J. Biol. Chem.* **272:** 7264–7277.

Desai, C. J., Gindhart, J. G., Jr., Goldstein, L. S. B., and Zinn, K. (1996). Receptor tyrosine phosphatases are required for motor axon guidance in the Drosophila embryo. *Cell* **84:** 599–609.

Desai, C. J., Krueger, N. X., Saito, H., and Zinn, K. (1997). Competition and cooperation among receptor tyrosine phosphatases control motoneuron growth cone guidance in Drosophila. *Development* **124:** 1941–1952.

Desai, C. J., Popova, E., and Zinn, K. (1994). A Drosophila receptor tyrosine phosphatase expressed in the embryonic CNS and larval optic lobes is a member of the set of proteins bearing the HRP carbohydrate epitope. *J. Neurosci.* **14:** 7272–7283.

Felberg, J., and Johnson, P. (1998). Characterization of recombinant CD45 cytoplasmic domain proteins—Evidence for intramolecular and intermolecular interactions. *J. Biol. Chem.* **273:** 17839–17845.

Garrity, P. A., Lee, C. H., Salecker, I., Robertson, H. C., Desai, C. J., Zinn, K., and Zipursky, S. L. (1999). Retinal axon target selection in *Drosophila* is regulated by a receptor protein tyrosine phosphatase. *Neuron* **22:** 707–717.

Haj, F., McKinnell, I., and A., S. (1999). Retinotectal ligands for the receptor tyrosine phosphatase CRYP alpha. *Mol. Cell Neurosci.* **14:** 225–240.

Hamilton, B. A., Ho, A., and Zinn, K. (1995). Targeted mutagenesis and genetic analysis of a *Drosophila* receptor-linked protein tyrosine phosphatase gene. *Roux's Arch. Dev. Biol.* **204:** 187–192.

Hariharan, I., Chuang, P.-T., and Rubin, G. M. (1991). Cloning and characterization of a receptor-class phosphotyrosine phosphatase gene expressed on central nervous system axons in *Drosophila melanogaster. Proc. Natl. Acad. Sci. USA* **88:** 11266–11270.

Hidalgo, A., and Brand, A. H. (1997). Targeted neuronal ablation—The role of pioneer neurons in guidance and fasciculation in the CNS of Drosophila. *Development* **124:** 3253–3262.

Hoffmann, K. M. V., Tonks, N. K., and Barford, D. (1997). The crystal structure of domain 1 of receptor protein-tyrosine phosphatase Mu. *J. Biol. Chem.* **272:** 27505–27508.

Jiang, G., den Hertog, J., Su, J., Noel, J., Sap, J., and Hunter, T. (1999). Dimerization inhibits the activity of receptor-like protein-tyrosine phosphatase-alpha. *Nature* **401:** 606–610.

Jiang, G. Q., den Hertog, J., and Hunter, T. (2000). Receptor-like protein tyrosine phosphatase alpha homodimerizes on the cell surface. *Mol. Cell. Biol.* **20:** 5917–5929.

Kennerdell, J. R., and Carthew, R. W. (1998). Use of dsRNA-mediated genetic interference to demonstrate that frizzled and frizzled 2 act in the wingless pathway. *Cell* **95:** 1017–1026.

Keshishian, H., Broadie, K., Chiba, A., and Bate, M. (1996). The *Drosophila* neuromuscular junction: A model for studying development and function. *Annu. Rev. Neurosci.* **19:** 545–575.

Kidd, T., Brose, K., Mitchell, K. J., Fetter, R. D., Tessier-Lavigne, M., Goodman, C. S., and Tear, G. (1998a). Roundabout controls axon crossing of the CNS midline and defines a novel subfamily of evolutionarily conserved guidance receptors. *Cell* **92:** 205–215.

Kidd, T., Russell, C., Goodman, C. S., and Tear, G. (1998b). Dosage-sensitive and complementary functions of roundabout and commissureless control axon crossing of the CNS midline. *Neuron* **20:** 25–33.

Krueger, N. X., Van Vactor, D., Wan, H. I., Gelbart, W. M., Goodman, C. S., and Saito, H. (1996). The transmembrane tyrosine phosphatase DLAR controls motor axon guidance in Drosophila. *Cell* **84:** 611–622.

Maeda, N., K., I..-T., T., K., Kadomatsu, K., Muramatsu, T., and Noda, M. (1999). A receptor-like protein-tyrosine phosphatase PTP zeta/RPTP beta binds a heparin-binding growth factor midkine—Involvement of arginine 78 of midkine in the high affinity binding to PTP zeta. *J. Biol. Chem.* **274:** 12474–12479.

Maeda, N., Nishiwaki, T., Shintani, T., Hamanaka, H., and Noda, M. (1996). 6B4 proteoglycan/phosphacan, an extracellular variant of receptor-like protein-tyrosine phosphatase zeta/RPTP beta, binds pleiotrophin/heparin-binding growth-associated molecule (HB-GAM). *J. Biol. Chem.* **271:** 21446–21452.

Majeti, R., Bilwes, A. M., Noel, J. P., Hunter, T., and Weiss, A. (1998). Dimerization-induced inhibition of receptor tyrosine phosphatase function through an inhibitory wedge. *Science* **279:** 88–91.

Meng, K., Rodriguez-Pena, A., Dimitrov, T., Chen, W., Yamin, M., Noda, M., and Devel, T. F. (2000). Pleiotrophin signals increased tyrosine phosphorylation of beta-catenin through inactivation of the intrinsic catalytic activity of the receptor-type protein tyrosine phosphatase beta/zeta. *Proc. Natl. Acad. Sci. USA* **97:** 2603–2608.

Misquitta, L., and Paterson, B. M. (1999). Targeted disruption of gene function in Drosophila by RNA interference (RNA-i): A role for nautilus in embryonic somatic muscle formation. *Proc. Natl. Acad. Sci. USA* **96:** 1451–1456.

Nam, H. J., Poy, F., Krueger, N. X., Saito, H., and Frederick, C. A. (1999). Crystal structure of the tandem phosphatase domains of RPTP LAR. *Cell* **97:** 449–457.

Newsome, T. P., Asling, B., and Dickson, B. J. (2000). Analysis of Drosophila photoreceptor axon guidance in eye-specific mosaics. *Development* **127:** 851–860.

O'Grady, P., Thai, T. C., and Saito, H. (1998). The laminin–nidogen complex is a ligand for a specific splice isoform of the transmembrane protein tyrosine phosphatase LAR. *J. Cell Biol.* **141:** 1675–1684.

Oon, S. H., Hong, A., Yang, X. H., and Chia, W. (1993). Alternative splicing in a novel tyrosine phosphatase gene (DPTP4E) of Dro-

sophila-melanogaster generates 2 large receptor-like proteins which differ in their carboxyl termini. *J. Biol. Chem.* **268:** 23964–23971.

Patel, N. H. (1994). Imaging neuronal subsets and other cell types in whole-mount Drosophila embryos and larvae using antibody probes. In *Drosophila melanogaster: Practical Uses in Cell and Molecular Biology* (E. Fyrberg and L. S. B. Goldstein, Eds.), Vol. 44, pp. 446–488. Academic Press, San Diego.

Peles, E., Nativ, M., Campbell, P. L., Sakurai, T., Martinez, R., Lev, S., Clary, D. O., Schilling, J., Barnea, G., Plowman, G. D., *et al.* (1995). The carbonic anhydrase domain of receptor tyrosine phosphatase β is a functional ligand for the axonal cell recognition molecule contactin. *Cell* **82:** 251–260.

Revest, J., Faivre-Sarrailh, C., Maeda, N., Noda, M., Schachner, M., and Rougon, G. (1999). The interaction between F3 immunoglobulin domains and protein tyrosine phosphatases zeta/beta triggers bidirectional signalling between neurons and glial cells. *Eur. J. Neurosci.* **11:** 1134–1147.

Rorth, P., Szabo, K., Bailey, A., Laverty, T., Rehm, J., Rubin, G. M., Weigmann, K., Milan, M., Benes, V., Ansorge, W., *et al.* (1998). Systematic gain-of-function genetics in Drosophila. *Development* **125:** 1049–1057.

Schmid, A., Chiba, A., and Doe, C. Q. (1999). Clonal analysis of Drosophila embryonic neuroblasts: Neural cell types, axon projections, and muscle targets. *Development* **126:** 4653–4689.

Seeger, M., Tear, G., Ferres-Marco, D., and Goodman, C. S. (1993). Mutations affecting growth cone guidance in Drosophila: Genes necessary for guidance toward or away from the midline. *Neuron* **10:** 409–426.

Streuli, M., Krueger, N. X., Tsai, A. Y. M., and Saito, H. (1989). A family of receptor-linked protein tyrosine phosphatases in humans and *Drosophila. Proc. Natl. Acad. Sci. USA* **86:** 8698–8702.

Sun, Q., Bahri, S., Schmid, A., Chia, W., and Zinn, K. (2000). Receptor tyrosine phosphatases regulate axon guidance across the midline of the Drosophila embryo. *Development* **127:** 801–812.

Tian, S.-S., Tsoulfas, P., and Zinn, K. (1991). Three receptor-linked protein-tyrosine phosphatases are selectively expressed on central nervous system axons in the *Drosophila* embryo. *Cell* **67:** 675–685.

Van Vactor, D., Sink, H., Fambrough, D., Tsoo, R., and Goodman, C. S. (1993). Genes that control neuromuscular specificity in Drosophila. *Cell* **73:** 1137–1153.

Wallace, M. J., Fladd, C., Batt, J., and Rotin, D. (1998). The second catalytic domain of protein tyrosine phosphatase delta (PTP delta) binds to and inhibits the first catalytic domain of PTP sigma. *Mol. Cell. Biol.* **18:** 2608–2616.

Wang, J., and Bixby, J. L. (1999). Receptor tyrosine phosphatase-delta is a hemophilic, neurite-promoting cell adhesion molecule for CNS neurons. *Mol. Cell. Neurosci.* **14:** 370–384.

Wills, Z., Bateman, J., Korey, C. A., Comer, A., and Van Vactor, D. (1999). The tyrosine kinase Abl and its substrate Enabled collaborate with the receptor phosphatase Dlar to control motor axon guidance. *Neuron* **22:** 301–312.

Yang, X., Seow, K. T., Bahri, S. M., Oon, S. H., and Chia, W. (1991). Two Drosophila receptor-like tyrosine phosphatase genes are expressed in a subset of developing axons and pioneer neurons in the embryonic CNS. *Cell* **67:** 661–673.

Zinn, K., and Sun, Q. (1999). Slit branches out: A secreted protein mediates both attractive and repulsive axon guidance. *Cell* **97:** 1–4.

Zipursky, S., Venkatesh, T., Teplow, D. B., and Benzer, S. (1984). Neuronal development in the Drosophila retina: Monoclonal antibodies as molecular probes. *Cell* **36:** 15–26.

Zondag, G. C. M., Koningstein, G. M., Jiang, Y.-P., Sap, J., Moolenaar, W. H., and Gebbink, M. F. B. (1995). Homophilic interactions mediated by receptor tyrosine phosphatases μ and κ. *J. Biol. Chem.* **270:** 14247–14250.

Received June 16, 2000
Revised November 15, 2000
Accepted November 20, 2000
Published online January 19, 2001